Volume Element Method for Thermal Analysis of Superconducting DC Transmission Cable

Dimitrios I. Doukas, *Student Member, IEEE*, Andreas I. Chrysochos, *Member, IEEE*, Theofilos A. Papadopoulos, *Member, IEEE*, Dimitris P. Labridis, *Senior Member, IEEE*, Lennart Harnefors, *Fellow, IEEE*, and Giovanni Velotto

***Abstract*—The ever increasing need for cost-efficient, high-density power transmission brought to the fore applied superconductivity as an alternative worth investigating. Especially, high-temperature superconducting (HTS) dc cables emerge as a promising solution for bulk power transmission and their use in the near future is expected to be increased. HTS cables have the special characteristic of varying performance under different critical conditions, especially under different operating temperatures. Therefore, detailed thermal analysis of HTS cables representing thermodynamics and heat transfer for varying length and time is of significant importance. The analytical mathematical formulation presented in this paper solves heat transfer equations for a two-dimensional axisymmetric cable model and identifies temperature distribution over length and time. The analysis is conducted on a bipolar cable suggested by the Electric Power Research Institute for long-distance HTS dc transmission, while both steady-state and transient scenarios are examined.**

***Index Terms*—Bipolar dc cable, critical length, superconducting transmission, thermal modeling, volume element method.**

I. Introduction

TECHNOLOGY achievements over the last years, such as new voltage-source converter (VSC) topologies, resulted in an increasing adoption of dc for electric power transmission, especially for bulk amounts of power and long distances [1]. Although significant losses due to semiconductors occur, the advantages of VSCs e.g., increased controllability and bi-directional power transfer capability enabled them as the main solution for dc transmission. However, the discovery of high temperature superconductivity [2] enabled moving on the next step, since replacement of conventional transmission by HTS cables is presented as an alternative that can lead to almost loss-less transmission, due to their nearly zero resistance [3].

Manuscript received September 2, 2016; accepted January 1, 2017. Date of publication January 20, 2017; date of current version February 10, 2017.

D. I. Doukas, A. I. Chrysochos, and D. P. Labridis are with the School of Electrical and Computer Engineering, Aristotle University of Thessaloniki, Thessaloniki 54124, Greece (e-mail: doux@auth.gr; anchryso@auth.gr; labridis@auth.gr).

T. A. Papadopoulos is with the Power Systems Laboratory, Department of Electrical and Computer Engineering, Democritus University of Thrace, Xanthi 67100, Greece (e-mail: thpapad@ee.duth.gr).

L. Harnefors and G. Velotto are with ABB Corporate Research, Västerås 72178, Sweden (e-mail: lennart.harnefors@se.abb.com; giovanni.velotto@se.abb.com).

Color versions of one or more of the figures in this paper are available online at http://ieeexplore.ieee.org.

Digital Object Identifier 10.1109/TASC.2017.2656785

TABLE I
Major HTS DC Transmission Projects

Project (Country)	l (m)	V (kV)	I (kA)
KEPRI (South Korea) [6]	100	80	3.25
CASER (Japan)[7]	200	10	2
IEE CAS (China) [8]	360	1.3	10
Jeju Island (South Korea) [9]	500	80	3.125
St. Petersburg (Russia) [10]	2500	20	2.5

Moreover, HTS cables can contribute to lighter and more compact power equipment for next generation all-electric ships and aircraft [4].

In Table I, a selection of HTS dc cable projects that attracted researchers' interest over the last decade is presented, revealing a trend of increasing transmission line lengths. Despite the proof of their technical feasibility, HTS cable installations are facing challenges to be massively adopted within the power grid due to techno-economic issues, such as complexity, low damping, increased capital and operational costs as well as the need for a reliable and cost-efficient cooling system [4], [5].

Analytic formulations, modeling approaches and computational tools are becoming significantly important for the design and analysis of large-scale superconducting power equipment [11]. Given the rarity of experimental installations and prototypes, numerical models have gained ground as popular tools to examine electromagnetic, thermal or coupled behavior of superconducting equipment [12], [13]. Robust and reliable tools can help to define the operation framework, predict limitations [11], deal with coupled problems, such as mechanical-thermal [14] or magneto-thermal [15], and reduce considerably the overall cost or increase reliability during operation [11].

Most modeling methodologies focus on the electromagnetic behavior of HTS equipment mainly for optimization purposes in order to simulate their performance under variable conditions, geometries and material properties [12], [13]. Additionally, thermal analysis is of critical importance since it is vital to keep operating temperature within critical limits in order to maintain superconductivity and avoid quenching [16].

A literature survey on thermal modeling for HTS cables revealed that first attempts are tracked back in 1970s-80s with simplified 1D flow models to study stability and quenching [17]. Later, more sophisticated simulation tools in parallel with experimental validation studied quenching [18], heat-transfer stability

[19], temperature dispersion [20] and heat transfer on structures [21]. A detailed presentation of modeling tools over the years can be found in [11]. During the last decade, researchers have adopted the finite-element method (FEM) for thermal modeling. In [22] non-linear time-dependent FEM for temperature distribution is presented, while in [23] and [24] 3D FEM models to analyze the thermal behavior of HTS cables are examined. Similarly to FEM, volume-element-method (VEM) analysis has been used in [25] and [26] to calculate temperature and pressure distribution under different conditions. In these works, Newton-Raphson and Runge-Kutta methods are used for the steady-state and transient numerical solution, respectively. Finally, recent efforts on the same topic use multi-physics software as COMSOL [27], 4-C code [28] or thermal network methods (TNM) to determine temperature distribution over superconducting power equipment[4].

The scope of this paper is to present an alternative and accurate methodology in the area of thermal modeling for HTS cables by applying VEM methodology and using the flexible parabolic-elliptic partial differential equations (PDEPE) solver [29] of MATLAB [30]. Temperature and pressure profile for all cable layers is determined for varying time and space by solving a coupled system of partial differential equations based on thermodynamic and heat transfer laws. Heat transfer by conduction, convection and radiation is considered, and the analysis is applied on an HTS dc cable resulted from Electric Power Research Institute (EPRI) studies [31], [32]. Mathematical formulation is presented and a set of scenarios, such as steady-state operating conditions, thermal transient response and critical length estimation are examined.

The contribution of this paper is to extend a model developed in [25] and to combine it with an efficient solver to systematically investigate the effects of variations in flow rates, coolant flow directions, and critical length in a long HTS transmission cables. This paper proposes a generic and accurate model, based on VEM, that can be used as an efficient simulation and design tool to analyze any type of HTS cable. The proposed model predicts thermal behavior for both steady-state and transient conditions and can be useful to identify the cable critical length above which secure operation may be questioned. Finally, the proposed model can be part of a control implementation that deals with heat anomalies based on varying conditions.

In Section II, the problem formulation and the generic expressions form are presented. In Section III, VEM analysis, mathematical formulation as well as the cable under study are presented. Section IV presents assumptions, input variables, properties and conditions for the examined cable. In Section V, results are presented for different both steady-state and transient scenarios. Finally, Section VI concludes the paper.

II. Problem Formulation

The partial differential equations (PDEs) representing thermodynamics and heat transfer laws are written in the form of (1) and are introduced to the PDEPE solver of MATLAB. PDEPE solver deals with initial-boundary value problems for varying space x and time t

$$c\left(x,t,u,\frac{\partial u}{\partial x}\right)\frac{\partial u}{\partial t}=x^{-m}\frac{\partial}{\partial x}\left[x^{m}f\left(x,t,u,\frac{\partial u}{\partial x}\right)\right]+s\left(x,t,u,\frac{\partial u}{\partial x}\right). \tag{1}$$

All PDEs hold for $t_0 \le t \le t_f$ and $a \le x \le b$, where t_0 and t_f represent the start and end time of simulation, while a and b represent the sending and receiving end of the cable. m corresponds to the symmetry and can be 0, 1 or 2 for slab, cylindrical or spherical symmetry, respectively. Considering the numerical solution of (1), it is important to define the vector functions of flux $f(x,t,u,\frac{\partial u}{\partial x})$ and source $s(x,t,u,\frac{\partial u}{\partial x})$ terms. The coupling of the partial derivatives with respect to time is restricted by multiplying with a diagonal matrix $c(x,t,u,\frac{\partial u}{\partial x})$, with diagonal elements either zero for elliptic equations or positive for parabolic equations [29].

Initial conditions for the simulation start $t = t_0$ and all x, i.e., over the whole length, are given by equation (2)

$$u(x,t_0)=u_0(x). \tag{2}$$

Boundary conditions for all t and for one of the cable terminations, a or b, are determined by equation (3) and are expressed in terms of the flux term f. Therefore, two boundary conditions are introduced for the whole timespan, one for $x = a$ and one for $x = b$. Vector functions p and q are both time and space dependent, whereas only p may depend also on u. The elements of q are either identically zero or never zero.

$$p(x,t,u)+q(x,t)f\left(x,t,u,\frac{\partial u}{\partial x}\right)=0. \tag{3}$$

Scalars x and t are considered as inputs, while vectors u and $\frac{\partial u}{\partial x}$ represent the solution u and its partial derivative with respect to x, respectively. The solution u for the thermal problem is the temperature distribution for varying space and time. PDEPE calculates temperature distribution over space and time for all finite volume elements (VEs) of any layer. As initial conditions in this work, temperature at $t = t_0$ and all x for cable layers is considered. Boundary conditions are introduced for the coolant layers and depend on the coolant flow scenario examined. In case of parallel direction coolant flow from a to b, both $p(a,t)$ and $p(b,t)$ have a fixed temperature value and a zero value, respectively, whereas $q(a,t)$ for both layers is zero and $q(b,t)$ is unity. In case of opposite direction coolant flow, one of $p(a,t)$ and $p(b,t)$ has a fixed temperature value and the other is zero. $q(a,t)$ and $q(b,t)$ are either zero or unity for the corresponding cases.

III. VEM Analysis

VEM analysis divides cable layers in finite volumes using cylindrical coordinates for simultaneous discretization over time and space. Energy equations in terms of thermodynamics and heat transfer are solved in order to identify the variation of properties, such as temperature and liquid coolant pressure, over the cable length and time. The analysis that follows results in

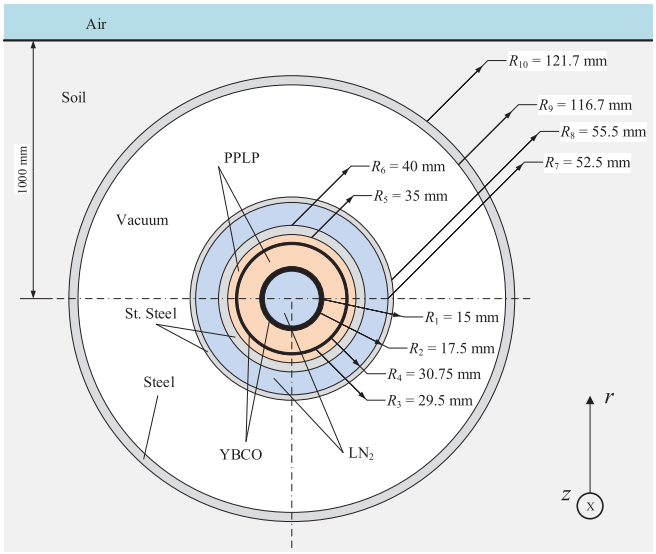

Fig. 1. HTS cable cross-section.

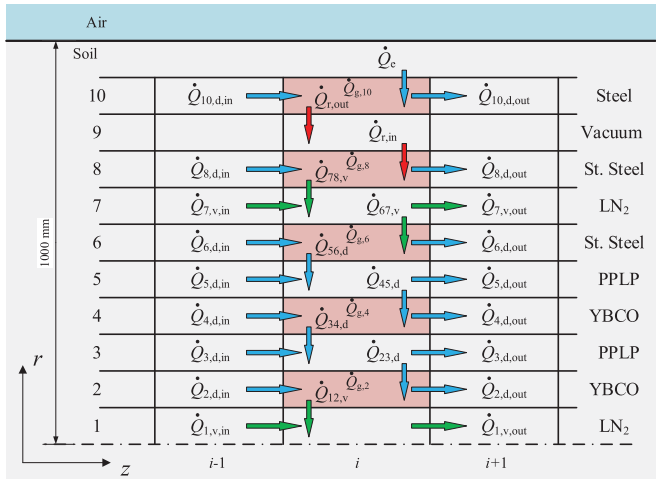

Fig. 2. Heat transfer and volume element discretization.

a system of PDEs representing heat transfer, between VEs in r and z directions.

The cable geometry studied in this paper is based on a project conducted by EPRI focused on long-distance, high-power HTS dc transmission [31]. For brevity, a simplified version of the inner part cross-section (fewer layers) of the cable, adopted also by EPRI in [32], was selected in the analysis. However, the mathematical formulation can be easily extended and applied to any cross-section regardless complexity. The cable cross-section is illustrated in Fig. 1. In contrast to previous studies [25], [26], that examine monopolar cables with gaseous helium as coolant, the geometry studied here is bipolar, which enables bidirectional power transfer with one cable and utilizes liquid nitrogen (LN_2) as coolant. This geometry results in a more cost-efficient approach, since the cooling circuit is the same for both power flow directions [33]. Yttrium barium copper oxide (YBCO) is considered as the HTS material, while polypropylene laminated paper (PPLP) is used for insulation. Thermal management and coolant flow issues are investigated in [34], [35] and addressed in Section V.

Regarding the mathematical formulation, expressions describing heat transfer conduction, convection and radiation are used. In Fig. 2 heat transfer reference directions are represented by arrows between consecutive volumes on both r and z directions. The discretization approach as shown in Fig. 2 as well as the heat transfer model expressed by equations (4)–(10) are based in the analysis of [25]. Note that the flux term f of (1) represents heat transfer on z direction, while the source term s the respective heat transfer on r direction.

A. Conduction

Between two consecutive VEs of solid materials heat transfer by conduction on both radial and axial directions takes place. Heat transfer by conduction is represented in Fig. 2 by blue color arrows. The expressions for heat conduction in $i-1$, i and $i+1$ consecutive VEs of the l^{th} cable layer, all consisting of the same material with thermal conductivity k_l, of a cross-section $A_{r,l}$ on z direction are given by

$$\begin{cases} \dot{Q}^i_{l,d,\text{in}} = -\dfrac{k_l A_{r,l}(T^i_l - T^{i-1}_l)}{\Delta^{i-1}_z} \\ \dot{Q}^i_{l,d,\text{out}} = -\dfrac{k_l A_{r,l}(T^{i+1}_l - T^i_l)}{\Delta^{i+1}_z}. \end{cases} \tag{4}$$

Similarly, the expressions for heat conduction for consecutive VEs of the i^{th} cable cross-section between different l_1 and l_2 cable layers, on r direction are given by

$$\dot{Q}^i_{l_1 l_2,d} = U^i_{l_1 l_2}(T^i_{l_2} - T^i_{l_1}) \tag{5}$$

where $U^i_{l_1 l_2}$ is

$$U^i_{l_1 l_2} = \left(\frac{\ln \frac{2R_{l_1}}{R_{l_1-1}+R_{l_1}}}{2\pi k_{l_1}\Delta^i_z} + \frac{\ln \frac{R_{l_1}+R_{l_2}}{2R_{l_1}}}{2\pi k_{l_2}\Delta^i_z} \right)^{-1} \tag{6}$$

where R_{l_1}, R_{l_2} and R_{l_1-1} are the radii of layers l_1, l_2 and of the inner layer before l_1, respectively.

B. Convection

Heat transfer by convection exists also both on the r and z directions between different solid and liquid materials and is represented by green color arrows in Fig. 2. Heat convection for consecutive VEs on z and r directions is given by

$$\begin{cases} \dot{Q}^i_{l,v,\text{in}} = -\dot{m}_l c_{p_l}(T^i_l - T^{i-1}_l) \\ \dot{Q}^i_{l,v,\text{out}} = -\dot{m}_l c_{p_l}(T^{i+1}_l - T^i_l) \end{cases} \tag{7}$$

$$\dot{Q}^i_{l_1 l_2,v} = h_{l_1} A^i_{l_1,l_2}(T^i_{l_2} - T^i_{l_1}) \tag{8}$$

where for Nusselt number Nu and hydraulic diameter D_h, h_{l_1} equals

$$h_{l_1} = \frac{k_{l_1}\text{Nu}}{D_h}. \tag{9}$$

C. Radiation

Heat radiation occurs outside the cryogenic enclosure, as seen in Fig. 2 with red arrows, as also in [25], [31], where vacuum is imposed. Heat radiation for consecutive VEs of the i^{th} cable cross-section between different l_1 and l_2 cable layers, that surround vacuum layer, on r direction is given by

$$\begin{cases} \dot{Q}^i_{r,\text{in}} = -\frac{\varepsilon_{l_1}}{1-\varepsilon_{l_1}} A^i_{l_1} \left[B_1 - \sigma (T^i_{l_1})^4\right] \\ \dot{Q}^i_{r,\text{out}} = -\frac{\varepsilon_{l_2}}{1-\varepsilon_{l_2}} A^i_{l_2} \left[\sigma (T^i_{l_2})^4 - B_2\right] \end{cases} \tag{10}$$

where σ is the Stefan-Boltzmann constant, ε is the material emissivity and B_1 and B_2 are determined in [25].

D. Heat Generation

In the proposed formulation the only heat source is the surrounding environment of the cable and is represented by $\dot{Q}_e$. Therefore, heat is transferred from soil inwards. Although, under steady-state conditions and within superconductivity critical limits no heat is expected to be generated on the HTS layers, sudden loss of superconductivity or induced currents on any conducting layer l may generate additional heat represented by $\dot{Q}_{g,l}$. In this case, heat transfer due to both sources, $\dot{Q}_e$ and $\dot{Q}_{g,l}$, will occur.

E. Pressure Calculation

For pressure drop calculations in both LN_2 channels, either laminar or turbulent flow can be considered depending on the Reynolds number Re as well as on construction characteristics, such as corrugations. The following expression is used

$$P^{i+1} = P^i - f \frac{\Delta z^i}{D_h} \frac{\rho^i (V^i)^2}{2} \tag{11}$$

where f, depending the flow type, equals to

$$\begin{cases} f = \frac{64}{\text{Re}} (\text{laminar}) \\ f = 4 \times 1.53 (\phi)^{0.46} \text{Re}^{-0.16} (\text{turbulent}). \end{cases} \tag{12}$$

For Re lower than 2000 laminar flow is assumed, whereas for Re larger than 4000 turbulent flow occurs. P, D_h, ρ and V represent the pressure, the hydraulic diameter and the LN_2 density and velocity, respectively. Last, ϕ is the sensitivity index that equals $\phi = h^2/(pD_h)$, where h and p represent the roughness height and the helical pitch, respectively. In this paper, ϕ and Re were taken equal to $0.8 \cdot 10^{-3}$ and 8000, respectively, based on [26], resulting in turbulent flow for both LN_2 channels.

F. EPRI Cable Modeling

For the cable cross-section and the heat transfer representation illustrated in Figs. 1 and 2, respectively, PDEs that represent the application of the first law of thermodynamics are derived for the i^{th} VE of all cable layers. Although the cable consists of 10 layers, only 9 PDEs are presented, since perfect vacuum was considered for the 9^{th} layer. All PDEs are expressed in the form of (1), in which on the left side of the equation is the coupling term c, whereas on the right side the flux f and source s terms, respectively. Heat transfer on the z axis, i.e., $\dot{Q}^i_{l,d,\text{in}}$, $\dot{Q}^i_{l,d,\text{out}}$, $\dot{Q}^i_{l,v,\text{in}}$ and $\dot{Q}^i_{l,v,\text{out}}$ represent the flux term f. Heat transfer on the r axis, i.e., $\dot{Q}^i_{l_1 l_2,d}$, $\dot{Q}^i_{l_1 l_2,v}$, $\dot{Q}^i_{r,\text{in}}$, $\dot{Q}^i_{r,\text{out}}$ and $\dot{Q}_e$ represent the source term s. Heat generation on conductors, expressed as $\dot{Q}_{g,l}$, is also part of the source term s. Expressions that represent the temperature distribution over space and time for the examined cable configuration can be found in detail in the Appendix.

TABLE II
MATERIAL PROPERTIES AND INITIAL CONDITIONS

Material	k (W/mK)	ρ (kg/m^3)	c_v (J/kgK)	c_p (J/kgK)	T_{init} (K)
LN_2 (1, 7)	0.026	808	742	1040	66
YBCO (2, 4)	208.45	8800	300	–	73
PPLP (3, 5)	0.05	946	600	–	93
St. Steel (6, 8)	9.4	7600	200	–	93
Steel (10)	16	7800	500	–	299

TABLE III
COMPUTATIONAL BURDEN FOR VARYING DISCRETIZATION

Space Segments \ Time Segments	864	8640	86400
30	18 s	25 s	49 s
300	190 s	265 s	525 s
3000	2026 s	2820 s	5598 s

IV. ASSUMPTIONS AND CONSTRAINTS

For HTS cable layers 2 and 4 of Fig. 1 through which current flows under steady-state conditions, YBCO is considered as the HTS material, while PPLP is used as insulation material for layers 3 and 5. PPLP is selected because it maintains stable insulation characteristics, high dielectric strength and low dielectric loss even at cryogenic temperatures. Thermodynamic properties of YBCO were considered as functions of temperature for a more realistic approach [36]. LN_2 was chosen as the coolant, and its thermodynamic properties were expressed as functions of temperature and pressure.

Regarding the discretization over space and time, respectively, 300 VEs were considered for the 100-m cable length and 8640 time segments for 1-day period, i.e., 1 time segment corresponds for 10 s. Furthermore, the index i can take values from 1 to 9 since the layer of vacuum is not considered in the analysis, therefore the temperature distribution for the remaining 9 cable layers is calculated. For the given discretization setup, the computational burden is 265 s, using an Intel Core i7-5500U, 2.4 GHz, RAM 8 GB personal computer, using MATLAB. Note that, as is evident by Table III, increasing the discretization for the same 100-m cable length, especially over space, will increase the computational burden exponentially. Therefore, for transient scenarios, domain discretization can be also applied with an irregular grid and varying Δz in order to increase VEs at the area of importance, e.g., a hot spot.

Different LN_2 flow scenarios were studied in order to identify the most efficient solution. Mass flow of LN_2 was taken equal to 3 kg/s based on [31]. The initial pressure on both LN_2 channels,

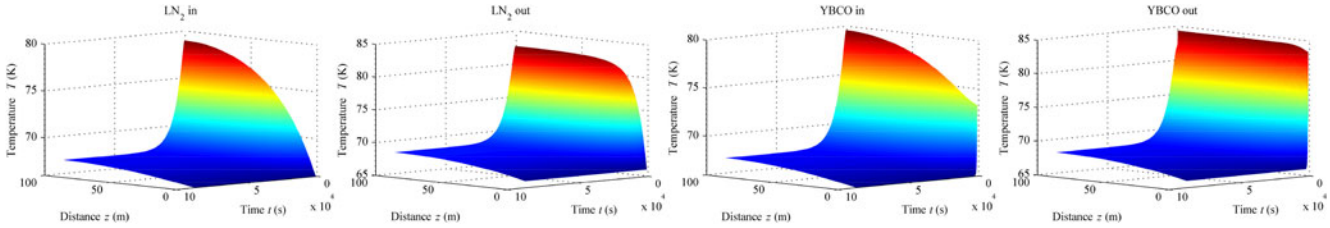

Fig. 3. Operating conditions and temperature distribution for internal LN_2 channel, internal and external HTS layers.

regardless the scenario examined, is taken equal to 30 atm, based on [31]. The cable armor and the cryogenic enclosure pipe are made of stainless steel due to the low temperatures whereas the outside cable pipe is made of steel. Details on the material properties and the initial conditions T_{init} are given in Table II. The cable is buried 1 m underground, while soil temperature equals 300 K.

Although in commercial cables, additional layers for mechanical support or multi-layer insulation (MLI) usually exist, in the presented analysis are not considered. Furthermore, in order for the cable to keep its position, mechanical support is necessary, otherwise, the LN_2 circulation and the respective pressure drop are affected. Moreover, in this paper perfect symmetry is considered.

V. Results

Scenarios representing both steady-state as well as thermal transient operating conditions are examined. Cable energization, critical cable length, alternative coolant flow configurations and heat generation events are thermal analysis aspects that are addressed and discussed.

A. Operating Conditions

First, in Fig. 3, indicative operating conditions results for both coolant channels and HTS layers are presented. The scenario explored focuses on a 100-m cable for an 1-day simulation period. Furthermore, coolant flow of the same direction is imposed on both LN_2 channels. Note the long-lasting thermal transient for the HTS layers, shown in Fig. 3, since it takes several hours for the HTS materials to be frozen into temperatures lower than the critical ones and thus become superconducting. Furthermore, since the coolant flow is of the same direction for both channels, an increasing temperature on cable materials for longer lengths is observed as expected. Similar remarks and observations are recorded in [31], [35], verifying the validity of the proposed model. Moreover, in Fig. 4, the pressure drop curve across the cable is presented showing significant resemblance with the corresponding results in [31].

Finally, an important aspect of HTS thermal analysis is the heat leak per unit length that represents heat transferred to the cryogenic pipe by the outer pipe. In Fig. 5 heat leak in W/m is presented and results are similar to the corresponding of [37].

B. Coolant Mass Flow Variations

The aforementioned characteristic of increasing temperatures with cable length indicates that for the same conditions for a

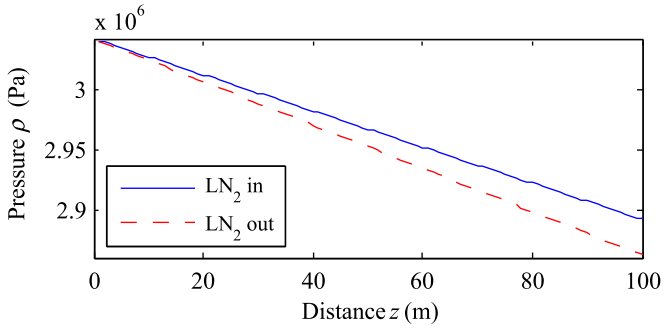

Fig. 4. Pressure drop for both LN_2 channels.

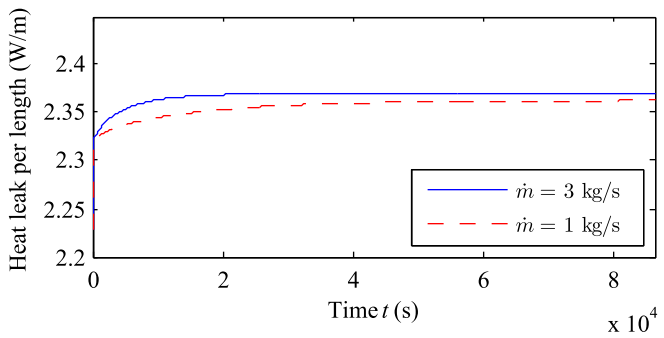

Fig. 5. Heat leak per unit length between cryogenic and outer pipe.

specific length, temperature of either HTS or coolant materials will inevitably exceed critical limits and the cable will be led to quenching. The critical temperature for YBCO is approximately 90 K, while nitrogen, for pressure up to 30 atm, is in the form of LN_2 between 63 and 123 K. To further investigate this behavior, a similar simulation setup was conducted, assuming a 300-m cable. As seen in Fig. 6, the temperature on the outer HTS layer increased by more than 10 K and tends gradually to 90 K. To deal with this issue, increase of the coolant mass flow can be helpful. In Fig. 7, the same scenario was examined for a coolant mass flow that equals 9 kg/s. It is clear that, exceeding critical limits may occur for longer distances, since for $\dot{m}$ equal to 9 kg/s the temperature was increased by only 4 K. Therefore, the model can be used to predict the temperature increase against cable length, to optimize the cooling system, to identify the distance between cooling stations or to appropriately control temperature with coolant flow.

C. Coolant Flow Directions

Instead of increasing the coolant mass flow $\dot{m}$ to deal with unacceptable temperature increase, alternative coolant

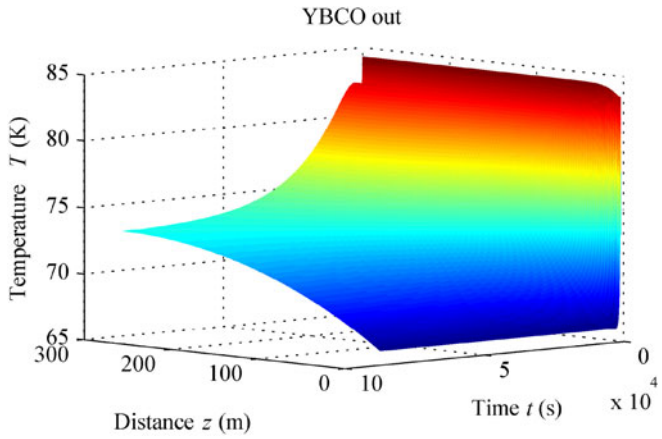

Fig. 6. Temperature distribution of the external HTS layer for $\dot{m} = 3$ kg/s.

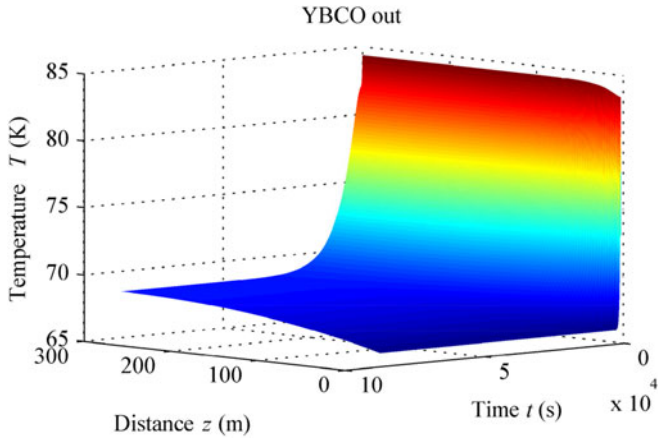

Fig. 7. Temperature distribution of the external HTS layer for $\dot{m} = 9$ kg/s.

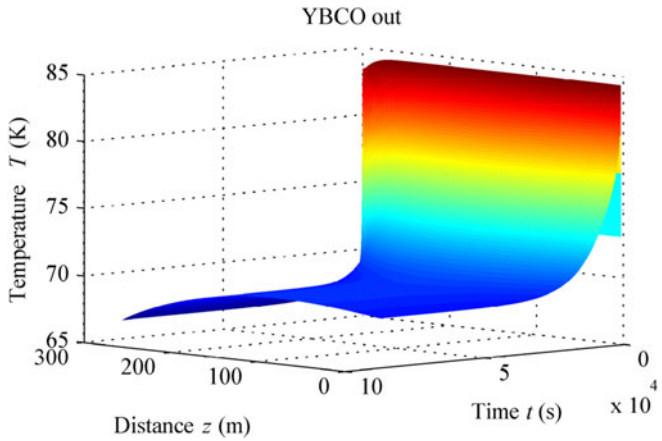

Fig. 8. Temperature of the external HTS - opposite coolant configuration.

configurations are examined. As suggested in [35], opposite - instead of same direction - coolant flow may improve the cable thermal performance. In Fig. 8, for the 300-m cable considered with initial mass flow 3 kg/s, the outer LN_2 is of opposite direction. It is evident how beneficiary for the transmission system this configuration can be. Claim presented in [35] about increasing temperature in the middle of the cable rather than

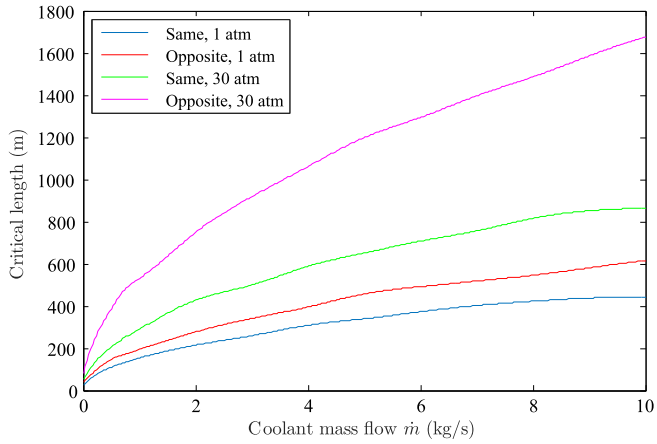

Fig. 9. Critical length for varying $\dot{m}$ and both coolant configurations.

in the termination points is also evident to further validate the model accuracy.

D. Critical Length

Combining both examined scenarios, maximum feasible length, i.e., critical length, for varying mass flow $\dot{m}$ and for both coolant configurations is investigated by a comprehensive analysis that has been conducted as seen in Fig. 9. Critical length is defined as the maximum length under which operation at temperatures that not exceed critical values for HTS and coolant materials is ensured. It is shown that for opposite coolant configurations longer cable lengths can be feasible for the same $\dot{m}$. However, from a mass flow $\dot{m}$ and onwards the critical length increases asymptotically. To reach longer cables, material properties, cross-section geometry and vacuum layer thickness need to be modified accordingly.

E. Heat Generation

Finally, heat generation on any conducting layer is an issue that needs to be taken into account by accurate thermal modeling. Heat may be generated on any conductor, because of currents on the HTS layers approaching or exceeding the critical limit, due to harmonics, induced currents, or temporary failures on the cooling system. In Fig. 10, a heat generation event at a cable segment on the outer YBCO layer that lasts 5000 s is presented. It is evident, that such an event increases the temperature of the HTS layer as well as of the surrounding layers. For higher in magnitude heat generation events, temperature on HTS or coolant layers will be affected and the cable may be led to quenching.

In Fig. 11, temperature over time at a specific cable segment is presented for different heat generation events, that last 5000 s, on the internal YBCO layer. Considering $\dot{m}$ equal to 3 kg/s, it is shown that for events of more than 200 W, temperature will exceed the critical limit. To deal with heat generation events, as in Fig. 11, increased coolant mass flow can be triggered in order to damp the thermal transient and ensure operation. Increasing the coolant flow will reduce temperature peaks and secure the

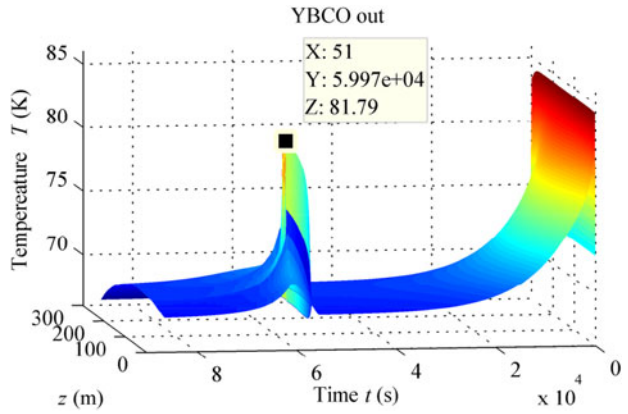

Fig. 10. Temperature distribution of the external HTS - heat generation event.

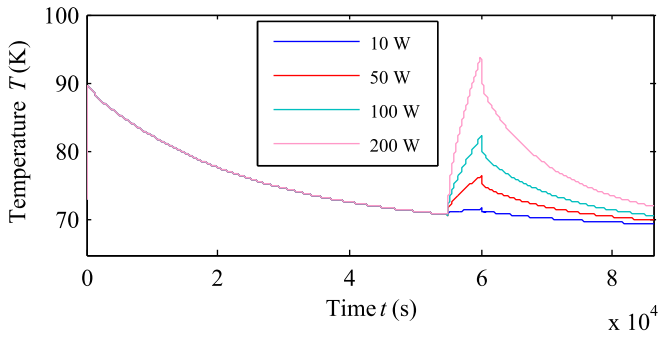

Fig. 11. Temperature of HTS for heat generation events and $\dot{m} = 3$ kg/s.

installation. Therefore, the proposed model can also be used as a thermal state estimator tool useful to control the cooling system.

VI. Conclusion

In this paper, a fully analytic mathematical formulation regarding thermal modeling, based on VEM analysis, of HTS cables was presented combined with an efficient numerical solution. VEM analysis and the discretization approach proposed in [25] are combined with an efficient solver to constitute an accurate simulation tool to systematically investigate HTS thermal behavior.

The proposed method is a useful tool to identify critical cable length limits, within which operation can be secured without exceeding critical values for both HTS and coolant materials. Same and opposite coolant flow directions are investigated revealing that the latter method is more effective in order to make feasible longer cable installations. The integration of pressure calculations in the proposed model can be used for cooling system sizing and the determination of distances between adjacent cooling substations. Finally, the proposed method can be incorporated in control systems that, in case of a detected failure, modify the coolant supply accordingly to damp thermal transients.

Results indicate that the model presents realistic results, close to existing literature, and that can be used to analyze the thermal behavior of the cable for varying time and space under different operating conditions. Conclusions to the actual design and fabrication of an HTS cable are listed as:

1) Temperature increase along the HTS cable can be reduced by appropriate tuning of the coolant mass flow $\dot{m}$.
2) Pressure drop along the HTS cable depends on flow type and on construction characteristics.
3) Critical length under which reliable operation is ensured is from 400 to 1800 m depending on the setup.
4) Opposite coolant flow directions make longer cable installations feasible.
5) Heat generation events can put superconducting state at risk and can be treated by appropriate coolant flow tuning.

Future extensions will include the development of a coupled electro-thermal model for HTS cables to investigate holistically the influence of all cable materials on the cable performance.

Appendix

The left side of the equations contains the coupling term c. The first two quantities on the right side of all equations (A.13)–(A.21) represent flux term f, while the remaining ones the source term s, as presented in Sections II and III.

$$\underbrace{\left(c_{v_{\mathrm{LN_2}}}\rho_{\mathrm{LN_2}}A_{r,1}\Delta_z^i\right)}_{\text{coupling } c}\frac{\partial T_1^i}{\partial t} = \underbrace{\dot{Q}_{1,v,\mathrm{in}}^i - \dot{Q}_{1,v,\mathrm{out}}^i}_{\text{flux } f} + \underbrace{\dot{Q}_{12,v}}_{\text{source } s} \tag{A.13}$$

$$\left(c_{v_{\mathrm{YBCO}}}\rho_{\mathrm{YBCO}}A_{r,2}\Delta_z^i\right)\frac{\partial T_2^i}{\partial t} = \dot{Q}_{2,d,\mathrm{in}}^i - \dot{Q}_{2,d,\mathrm{out}}^i - \dot{Q}_{12,v} + \dot{Q}_{23,d} + \dot{Q}_{g,2}^i \tag{A.14}$$

$$\left(c_{v_{\mathrm{PPLP}}}\rho_{\mathrm{PPLP}}A_{r,3}\Delta_z^i\right)\frac{\partial T_3^i}{\partial t} = \dot{Q}_{3,d,\mathrm{in}}^i - \dot{Q}_{3,d,\mathrm{out}}^i - \dot{Q}_{23,d} + \dot{Q}_{34,d} \tag{A.15}$$

$$\left(c_{v_{\mathrm{YBCO}}}\rho_{\mathrm{YBCO}}A_{r,4}\Delta_z^i\right)\frac{\partial T_4^i}{\partial t} = \dot{Q}_{4,d,\mathrm{in}}^i - \dot{Q}_{4,d,\mathrm{out}}^i - \dot{Q}_{34,d} + \dot{Q}_{45,d} + \dot{Q}_{g,4}^i \tag{A.16}$$

$$\left(c_{v_{\mathrm{PPLP}}}\rho_{\mathrm{PPLP}}A_{r,5}\Delta_z^i\right)\frac{\partial T_5^i}{\partial t} = \dot{Q}_{5,d,\mathrm{in}}^i - \dot{Q}_{5,d,\mathrm{out}}^i - \dot{Q}_{45,d} + \dot{Q}_{56,d} \tag{A.17}$$

$$\left(c_{v_{\mathrm{St.Steel}}}\rho_{\mathrm{St.Steel}}A_{r,6}\Delta_z^i\right)\frac{\partial T_6^i}{\partial t} = \dot{Q}_{6,d,\mathrm{in}}^i - \dot{Q}_{6,d,\mathrm{out}}^i - \dot{Q}_{56,d} + \dot{Q}_{67,v} + \dot{Q}_{g,6}^i \tag{A.18}$$

$$\left(c_{v_{\mathrm{LN_2}}}\rho_{\mathrm{LN_2}}A_{r,7}\Delta_z^i\right)\frac{\partial T_7^i}{\partial t} = \dot{Q}_{7,v,\mathrm{in}}^i - \dot{Q}_{7,v,\mathrm{out}}^i - \dot{Q}_{67,v} + \dot{Q}_{78,v} \tag{A.19}$$

$$\left(c_{v_{\mathrm{St.Steel}}}\rho_{\mathrm{St.Steel}}A_{r,8}\Delta_z^i\right)\frac{\partial T_8^i}{\partial t} = \dot{Q}_{8,d,\mathrm{in}}^i - \dot{Q}_{8,d,\mathrm{out}}^i - \dot{Q}_{78,v} + \dot{Q}_{r,\mathrm{in}} + \dot{Q}_{g,8}^i \tag{A.20}$$

$$\left(c_{v_{\mathrm{Steel}}}\rho_{\mathrm{Steel}}A_{r,10}\Delta_z^i\right)\frac{\partial T_{10}^i}{\partial t} = \dot{Q}_{10,d,\mathrm{in}}^i - \dot{Q}_{10,d,\mathrm{out}}^i - \dot{Q}_{r,\mathrm{out}} + \dot{Q}_e + \dot{Q}_{g,10}^i \tag{A.21}$$

REFERENCES

[1] N. Flourentzou, V. G. Agelidis, and G. D. Demetriades, "VSC-based HVDC power transmission systems: An overview," *IEEE Trans. Power Electron.*, vol. 24, no. 3, pp. 592–602, Mar. 2009.

[2] J. G. Bednorz and K. A. Muller, "Possible high Tc superconductivity in the Ba-La-Cu-O system," *Zeitschrift für Physik B Condensed Matter*, vol. 64, pp. 189–193, Apr. 1986.

[3] G. Venkataramanan and B. K. Johnson, "A superconducting DC transmission system based on VSC transmission technologies," *IEEE Trans. Appl. Supercond.*, vol. 13, no. 2, pp. 1922–1925, Jun. 2003.

[4] L. Graber, J. G. Kim, C. H. Kim, and S. V. Pamidi, "Thermal network model for HTS cable systems and components cooled by helium gas," *IEEE Trans. Appl. Supercond.*, vol. 26, no. 4, Jun. 2016, Art. no. 4803805.

[5] D. I. Doukas, Z. D. Blatsi, A. N. Milioudis, D. P. Labridis, L. Harnefors, and G. Velotto, "Damping of electromagnetic transients in a superconducting VSC transmission system," in *Proc. IEEE Eindhoven Power Tech*, Jun. 2015, pp. 1–6.

[6] B. Yang, J. Kang, S. Lee, C. Choi, and Y. Moon, "Qualification test of a 80 kV 500 MW HTS DC cable for applying into real grid," *IEEE Trans. Appl. Supercond.*, vol. 25, no. 3, Jun. 2015, Art. no. 5402705.

[7] M. Hamabe, H. Watanabe, J. Sun, N. Yamamoto, T. Kawahara, and S. Yamaguchi, "Status of a 200-meter DC superconducting power transmission cable after cooling cycles," *IEEE Trans. Appl. Supercond.*, vol. 23, no. 3, Jun. 2013, Art. no. 5400204.

[8] D. Zhang *et al.*, "Testing results for the cable core of a 360 m/10 kA HTS DC power cable used in the electrolytic aluminum industry," *IEEE Trans. Appl. Supercond.*, vol. 23, no. 3, Jun. 2013, Art. no. 5400504.

[9] J. H. Lim *et al.*, "Cryogenic system for 80-kV DC HTS cable in the KEPCO power grid," *IEEE Trans. Appl. Supercond.*, vol. 25, no. 3, Jun. 2015, Art. no. 5402804.

[10] V. E. Sytnikov *et al.*, "HTS DC cable line project: On-going activities in Russia," *IEEE Trans. Appl. Supercond.*, vol. 23, no. 3, Jun. 2013, Art. no. 5401904.

[11] L. Bottura, "Thermal, hydraulic, and electromagnetic modeling of superconducting magnet systems," *IEEE Trans. Appl. Supercond.*, vol. 26, no. 3, Apr. 2016, Art. no. 4901807.

[12] F. Grilli, E. Pardo, A. Stenvall, D. N. Nguyen, W. Yuan, and F. Gmry, "Computation of losses in HTS under the action of varying magnetic fields and currents," *IEEE Trans. Appl. Supercond.*, vol. 24, no. 1, Feb. 2014, Art. no. 8200433.

[13] F. Grilli, "Numerical modeling of HTS applications," *IEEE Trans. Appl. Supercond.*, vol. 26, no. 3, Apr. 2016, Art. no. 0500408.

[14] M. Watanabe *et al.*, "Thermo-mechanical properties of a 66 kV superconducting power cable system," *IEEE Trans. Appl. Supercond.*, vol. 13, no. 2, pp. 1956–1959, Jun. 2003.

[15] Z. Zhou *et al.*, "Magnetic-thermal coupling analysis of the cold dielectric high temperature superconducting cable," *IEEE Trans. Appl. Supercond.*, vol. 23, no. 3, Jun. 2013, Art. no. 5400404.

[16] G. P. Mikitik, Y. Mawatari, A. T. S. Wan, and F. Sirois, "Analytical methods and formulas for modeling high temperature superconductors," *IEEE Trans. Appl. Supercond.*, vol. 23, no. 2, Apr. 2013, Art. no. 8001920.

[17] V. Arp, "Stability and thermal quenches in force-cooled superconducting cables. Final report," National Bureau of Standards, Washington, DC, USA, Tech. Rep., 1979.

[18] C. A. Luongo, R. J. Loyd, F. K. Chen, and S. D. Peck, "Thermal-hydraulic simulation of helium expulsion from a cable-in-conduit conductor," *IEEE Trans. Magn.*, vol. 25, no. 2, pp. 1589–1595, Mar. 1989.

[19] A. Kamitani, T. Amano, S. Sekiya, and A. Ohara, "Stability analysis of a forced-flow cooled superconducting coil: Numerical simulation of multiple stability," *Cryogenics*, vol. 31, no. 2, pp. 110–118, 1991. [Online]. Available: http://www.sciencedirect.com/science/article/pii/001122759190256V

[20] L. Bottura and O. Zienkiewicz, "Quench analysis of large superconducting magnets. Part I: model description," *Cryogenics*, vol. 32, no. 7, pp. 659–667, 1992. [Online]. Available: http://www.sciencedirect.com/science/article/pii/001122759290299P

[21] A. Gavrilin, "Computer code for simulation of thermal processes during quench in superconducting magnets windings," *Cryogenics*, vol. 32, pp. 390–393, 1992. [Online]. Available: http://www.sciencedirect.com/science/article/pii/001122759290187F

[22] L. Rostila, J. Lehtonen, M. Masti, and R. Mikkonen, "Fault current model for YBCO cables," *Supercond. Sci. Technol.*, vol. 19, no. 8, pp. 756–761, 2006. [Online]. Available: http://stacks.iop.org/0953–2048/19/i=8/a=011

[23] J. He *et al.*, "Thermal analysis of HTS power cable using 3-D FEM model," *IEEE Trans. Appl. Supercond.*, vol. 23, no. 3, Jun. 2013, Art. no. 5402404.

[24] X. Wang *et al.*, "Thermal characteristics of 275 kV/3 kA class YBCO power cable," *IEEE Trans. Appl. Supercond.*, vol. 20, no. 3, pp. 1268–1271, Jun. 2010.

[25] J. A. Souza, J. C. Ordonez, R. Hovsapian, and J. V. C. Vargas, "Thermal modeling of helium cooled high-temperature superconducting DC transmission cable," *IEEE Trans. Appl. Supercond.*, vol. 21, no. 3, pp. 947–952, Jun. 2011.

[26] J. C. Ordonez, J. A. Souza, D. R. Shah, J. V. C. Vargas, and R. Hovsapian, "Temperature and pressure drop model for gaseous helium cooled superconducting DC cables," *IEEE Trans. Appl. Supercond.*, vol. 23, no. 3, Jun. 2013, Art. no. 5402005.

[27] N. Suttell, C. H. Kim, J. Ordonez, D. Shah, L. Graber, and S. Pamidi, "Thermal modeling of gaseous helium as a cryogen for high temperature superconducting cable components," *IEEE Trans. Appl. Supercond.*, vol. 25, no. 3, Jun. 2015, Art. no. 5401105.

[28] L. Savoldi *et al.*, "Thermal-hydraulic modeling of a novel HTS CICC for nuclear fusion applications," *IEEE Trans. Appl. Supercond.*, vol. 26, no. 3, Apr. 2016, Art. no. 4203407.

[29] R. D. Skeel and M. Berzins, "A method for the spatial discretization of parabolic equations in one space variable," *SIAM J. Sci. Statist. Comput.*, vol. 11, no. 1, pp. 1–32, 1990.

[30] *MATLAB, Version 8.2.0.701 (R2013b).* , The Math Works Inc., Natick, MA, USA, 2013.

[31] EPRI, "Program on technology innovation: A superconducting DC cable," EPRIPalo Alto, CA, USA, *Tech. Rep. 1020458*, Dec. 2009.

[32] EPRI "Program on technology innovation: Transient response of a superconducting DC long length cable system using voltage source converters," EPRI, Palo Alto, CA, USA, Tech. Rep. 1020339, Dec. 2009.

[33] P. Chowdhuri, C. Pallem, J. A. Demko, and M. J. Gouge, "Feasibility of electric power transmission by DC superconducting cables," *IEEE Trans. Appl. Supercond.*, vol. 15, no. 4, pp. 3917–3926, Dec. 2005.

[34] J. A. Demko and R. C. Duckworth, "Cooling configuration design considerations for long-length HTS cables," *IEEE Trans. Appl. Supercond.*, vol. 19, no. 3, pp. 1752–1755, Jun. 2009.

[35] J. A. Demko and W. V. Hassenzahl, "Thermal management of long-length HTS cable systems," *IEEE Trans. Appl. Supercond.*, vol. 21, no. 3, pp. 957–960, Jun. 2011.

[36] Y. Wang, *Fundamental Elements of Applied Superconductivity in Electrical Engineering*. Singapore: Wiley, 2013.

[37] J. Oestergaard, J. Okholm, K. Lomholt, and O. Toennesen, "Energy losses of superconducting power transmission cables in the grid," *IEEE Trans. Appl. Supercond.*, vol. 11, no. 1, pp. 2375–2378, Mar. 2001.